LETTER TO THE EDITOR

State Resolved Measurements of Single Electron Capture in Slow Ne^{7+} and Ne^{8+}–Helium Collisions

D Fischer†§, B Feuerstein†, R D Dubois‡, R Moshammer†, J R Crespo López–Urrutia†, I Draganic†, H Lörch†, A N Perumal† and J Ullrich†

† Max-Planck-Institut für Kernphysik, Heidelberg

‡ University of Missouri-Rolla

Abstract. Single electron capture in collisions of 9 keV$\times q$ Ne^{8+} and Ne^{7+} ions with He has been studied using cold-target recoil-ion momentum spectroscopy (COLTRIMS). With an improved apparatus a longitudinal momentum resolution of 0.07 a.u. has been achieved. This momentum component is directly proportional to the difference in the binding energy of the active electron between the final and the initial state. For the first time state-resolved differential cross sections have been determined with respect to the main quantum number, subshell level and spin state of the captured electron. A comparison with recent theoretical results for energy levels in Be-like neon is given.

Interactions of medium and highly charged ions with atoms or molecules are important in all areas of research employing low-density plasmas. These areas range from basic research studies where the goals are to understand plasmas and their properties to applications such as, e.g., nuclear fusion research or low-density plasmas in industry with regard to material modification. Interactions between ions and atoms or molecules have also developed new astrophysical importance since they are now recognized as being responsible for x-ray emission from comets [1]. Finally, in accelerator physics, these processes determine beam transport properties as well as lifetimes in storage rings. A common factor in all of these examples is charge exchange during interactions between low-energy ions and background gases. This process is of particular importance since its probability dramatically increases with the ion charge and it tends to lower the mean charge state and plasma temperature.

Another reason for investigating interactions of medium and high charge state ions with atoms or molecules is because they provide an excellent test for our understanding of atomic collision processes, dynamics, and atomic structure. Hence, these interactions have been studied since the advent of atomic collision physics in the previous century. Initial studies generally employed singly and doubly charged ions but the development of various highly charged ion sources during the past couple of decades have allowed studies to be performed for a wider and wider range of ion species. At lower impact

§ fischer@mpi-hd.mpg.de

energies which is the subject of this work, e.g., a few keV/amu or lower, numerous studies have shown that the predominant process is electron transfer from the target to the projectile. Also, it is known (for example, references [2–6]) that higher order processes occur where target or projectile excitation accompanies the electron transfer.

This information has been obtained by measuring the charge states, scattering angles, and energies of the projectile ions after interaction with gaseous targets. From the energy loss and scattering angles one obtains information about which states are populated and what impact parameters are involved. This method is generally restricted to low impact energies where the energy resolution is best and scattering angles are large. At higher energies, a series of measurements has been performed [7–12] where the longitudinal and transverse momenta of the recoil target ion produced in the interaction are measured. These momentum measurements also provide information about which states are populated and what impact parameters are important, i.e. information about the collision dynamics. For more details outlining the various methods and findings, the reader is referred to [2, 4, 13–15].

Theoretically, the impact parameters where the transfer takes place and the overall probabilities for populating various n levels can be predicted rather well with an 'over the barrier model' originally developed by Niehaus [16]. In addition, which states are populated can be determined by combining information about the impact parameter and molecular potential curves for the corresponding collision system. The Classical Trajectory Monte Carlo method also does a reasonable job in predicting probabilities for the population of various states, providing additional information about the interaction dynamics [17, 18], i.e. on the impact parameter dependence of the reactions.

In spite of the large number of experiments that have been performed in the past, particularly at impact energies of a few keV/amu and above, the limited energy resolutions allowed only in a few cases to obtain differential data about the final state ℓ levels population [6, 9, 14, 15]. Moreover, no experimental information regarding the dynamics involved in populating singlet and triplet states, which have been theoretically predicted [4] to differ, is available. Although photon emission has been used to achieve higher resolution [2, 19–21], possible cascade transitions complicate the interpretation of the data and limited solid angles for photon detection often inhibit studies of the collision dynamics. Another method of achieving higher resolution by employing MOT traps has been recently demonstrated [22, 23] but has not yet been applied to the study of collisions with highly charged ions.

The main motivation for the present study was to establish methods for performing recoil momentum measurements having 'spectroscopic' resolution. This is in line with future goals to use the former Freiburg Electron Beam Ion Trap (FreEBIT)‖ and a 'reaction microscope' [28] which, in combination, establish a unique tool to investigate interaction dynamics between highly charged ions and atomic or molecular targets.

For the present study, single electron capture for 9 keV $\times q$ Ne^{7+} and Ne^{8+} impact on

‖ FreEBIT has now been transferred to the Max-Planck-Institut für Kernphysik in Heidelberg, Germany

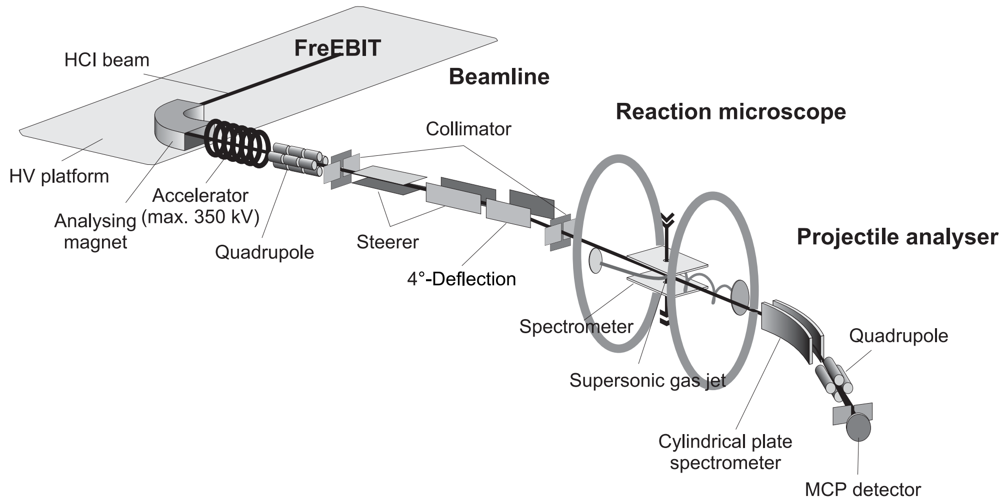

Figure 1. Schematic overview of the experimental setup. See text for details.

He was investigated since a) experimental and theoretical information about the neon ionic states is available [24–27], b) several close lying states requiring 'spectroscopic' resolution are populated, and c) the momentum transfer for these intermediate charge states and energies are sufficiently large to establish techniques which are required in future experiments employing very highly charged projectiles.

The whole experimental setup is shown in figure 1. It consists of the electron beam ion trap (EBIT) used as a source and a 'reaction microscope'. Ions extracted from the EBIT are charge-state and mass analysed by a 90° dipole magnet and directed through a beamline into the 'reaction microscope'. The beam is collimated and cleaned by a pair of slits and a 4° deflector.

After passing a well localized and cold beam of He-atoms provided by a three-stage supersonic gas jet the projectiles are charge-state analysed by a cylindrical-plate spectrometer and detected by a position-sensitive channel-plate detector. The 'reaction microscope' used is very similar to those, which have been described earlier [28]. The recoil ions are extracted along the projectile beam direction in order to achieve the best possible resolution for the longitudinal momentum component. They are accelerated over a distance of 11 cm by a weak electric field (1-5 V/cm) generated between two ceramic plates covered with resistive layers. To fulfil the time-focusing condition the recoil ions drift after acceleration through a field free region of 22 cm length and are detected by a position sensitive detector, which is placed just beneath the projectile beam axis (see figure 2). The He^{1+} momentum vector is calculated from the position on the recoil-ion detector and the time-of-flight measured in a coincidence between the recoil ion and the corresponding charge changed projectile.

For small projectile scattering angles the longitudinal momentum transfer, i. e. the recoil momentum along the projectile beam axis, depends only on the difference between the binding energies of the active electron in the initial and final state, i.e. on the Q-value of the reaction $p_{\|} = Q/v_{\mathrm{p}} - v_{\mathrm{p}}/2$ [1]. v_{p} is the projectile velocity. Thus,

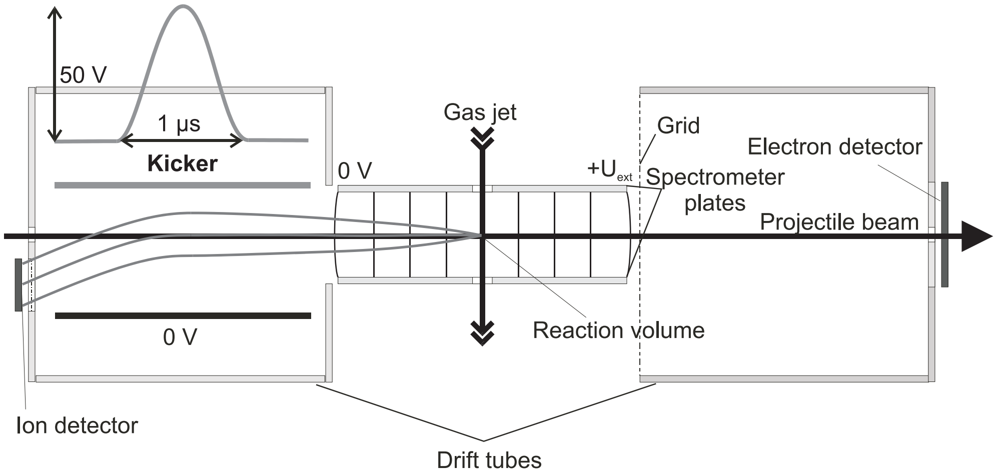

Figure 2. Schematic drawing of the 'reaction microscope' using a pulsed kicker giuding the recoil ions towards the off-axis ion detector.

the longitudinal momentum transfer allows to separate different shells populated in the capture reaction. The transverse recoil-ion momentum, on the other hand, reflects the projectile scattering angle ϑ via $p_\perp = \vartheta \cdot p_0$. The incoming projectile momentum is p_0. Hence, the full information about the collision dynamics and about populated electronic states is accessed via the precise measurement of the recoil-ion momentum vector.

The finally reachable momentum resolution is limited mainly by three factors. First, the major contribution comes from the thermal spread of the target, which amounts to $\Delta p = 0.26$ a.u. in the direction along the gas-jet axis and $\Delta p = 0.07$ a.u. perpendicular to it. Second, the spatial extension of the reaction volume which is determined by the overlap between ion beam and jet reduces the transverse momentum resolution. Due to the time-focusing geometry along the logituduinal direction this momentum component giving the Q-value is not noticeably affected by the finite target extension. The third contribution emerges from the uncertainty in the time-of-flight (TOF) measurement, which influences only the longitudinal momentum determination due to the orientation of the spectrometer along the projectile beam. The latter contribution is almost negligible for small extraction fields or large flight times of the recoil ions, respectively. Thus, longitudinal extraction is most suitable for the study of capture reactions allowing to achieve a very high resolution for the determination of the Q-value. With the present setup at an extraction voltage of 80 V a resolution of $\Delta p_\perp = 0.3$ a.u. and $\Delta p_{||} = 0.07$ a.u. was reached. For the projectile velocity used, this corresponds to a Q-value resolution of $\Delta Q_{\mathrm{FWHM}} = 0.7$ eV.

In order to reach this high resolution any deviation from ideal extraction conditions like e.g. electric fringe fields or non homogeneous electric fields for acceleration of the recoil ions have to be avoided. On the other hand, the longitudinal extraction geometry favourable due to the above-mentioned reasons requires a weak vertical component of the electric field to push the ions onto the off-axis recoil detector. This asymmetric potential gradient is easily generated by applying slightly different voltages to the upper and lower

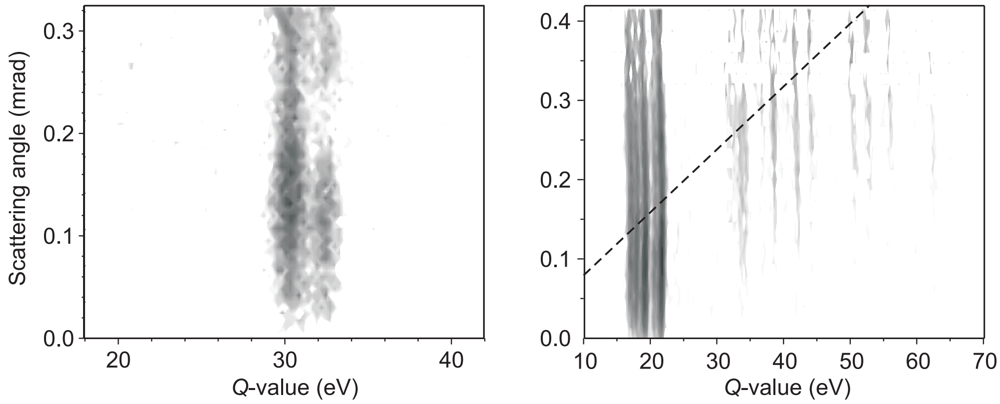

Figure 3. Two-dimensional spectra (scattering angle ϑ versus Q-value, log. scale) for single electron capture in Ne^{8+}- (a) and Ne^{7+}-He (b) collisions. The incident velocity is 0.38 a.u. and 0.355 a.u., respectively. In (b) the half Coulomb angle ϑ_C is shown as a broken line

spectrometer plates. For high-resolution studies, this technique has the disadvantage of mixing of transverse and longitudinal momentum components which results in a non-acceptable reduction of the momentum resolution to $\Delta Q_{\mathrm{FWHM}} = 1.25$ eV for Ne^{8+}, see Fig. 4(a).

To circumvent these problems arising from asymmetric extraction fields and to achieve the ultimate resolution, the recoil-ion drift tube was supplemented with an electrostatic kicker (fig. 2). It basically consists of two metallic plates where a transverse electric field can be generated by setting the plates on different voltages. Whenever a recoil ion passes these plates after extraction along the incoming ion beam it gets a kick in the transverse direction towards the recoil-ion detector by applying a short electric pulse. The timing of the kicker pulse is synchronized with the signal from the projectile analyzer, i.e. it is applied in coincidence to a capture reaction with a well defined time delay ensuring that each recoil ion experiences the field pulse at the same longitudinal position between the kicker plates. In the present experiment gaussian shaped 50 V pulses were used at a pulse width of 1 μs (the total time-of-flight was 11 μs). We note that arbitrarily shaped pulses can be used as long as their duration is considerably shorter than the recoil-ions transit time through the kicker. The improvement in resolution can be seen by comparing the Q-value spectra for Ne^{8+} and Ne^{7+} in Fig. 4(a) and 5(b), respectively. In the latter case, by means of the kicker, a resolution of $\Delta Q_{\mathrm{FWHM}} = 0.7$ eV was reached which is dominated by the thermal spread of the gas jet (see above).

In figure 3 the two-dimensional spectra (scattering angle ϑ versus Q-value) for single electron capture in Ne^{8+}- (a) and Ne^{7+}-He (b) collisions are shown. The incident velocity is 0.38 a.u. and 0.355 a.u., respectively.

The Q-value spectrum of Ne^{8+} exhibits a double-peak stucture (figure 4(a)) due to single capture into several $n = 4$ states of Li-like Ne^{7+}. The smaller line corresponds to the 4s state, whereas the other peak consists of three lines corresponding to the 4p,

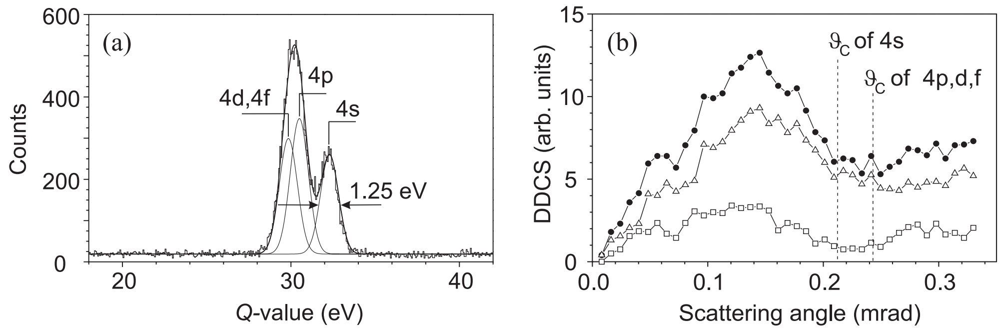

Figure 4. (a) Q-value spectrum and energy levels of Ne^{7+} following single electron capture from He at $v_p = 0.38$ a.u. (b) Differential capture cross sections (arb. units) for the two main components of spectrum (a): ● , total DDCS; □ $1s^2 4s$; △, $1s^2 4p$,d,f.

4d and 4f states. By means of a least squares fit to the data we get a decomposition of the spectrum as indicated in figure 4(a). Due to the finite resolution of 1.25 eV the 4d and 4f states could not be resolved. No indication for other transitions (as $n = 3$ or 5) was observed in the present experiment although $n = 5$ transitions have been found in fluorescence spectra [29]. The reason may be Auger transitions into $n = 5$ following double capture which cannot be distingiushed in the fluorescence experiment. Large scattering angles which are not accepted by our spectrometer are quite unlikely since $n = 5$ lies above $n = 4$. Within the curve-crossing picture this would lead to even smaller scattering angles. The curve-crossing model considers the potential curves of the collision system. In the case of a neutral target the incident channel is approximated by a constant function which can be set to zero whereas the final channel is given by a Coulombic potential curve for the two charged particles $E_C = q_1 q_2/r - Q + v_p^2/2$. Here, q_1, q_2 are the final charge states and r the distance between the particles. Acceleration of the transferred electron to the projectile velocity v_p is taken into account by the third term. The crossing radius where the charge transfer occurs is given by $r_{cc} = q_1 q_2/(Q - v_p^2/2)$. The deflection of the projectile undergoing capture at an impact parameter r_{cc} can be treated as a Coulombic 'half collision' which is given by the half Coulomb angle $\vartheta_C = Q/2E$, where E is the projectile energy. In figure 5(b) the differential capture cross sections for the two main components of spectrum 4(a) are presented. The curve for $1s^2 4s$ exhibits a distinct minimum around ϑ_C whereas for the other states a shoulder is observed at this point.

In contrast to the Ne^{8+} case, single capture in the Ne^{7+}–He collision leads to Be-like final states which give rise to a rich structure in the spectra, as shown in figures 3(b) and 5(a). In the latter a Q-value spectrum is presented which consists of three groups of lines corresponding to the $2s4\ell$ and $2s3\ell$ levels of Ne^{6+}, and to the doubly excited states $2p3\ell$. Projectile excitation accompaining the capture process has already been observed in a previous experiment [4] and possible mechanisms leading to transfer-excitation have been discussed therein. Unfortunately, the Q-value spectra in [4] suffer by the limited resolution. The improved resolution of 0.7 eV in the present experiment allows to resolve

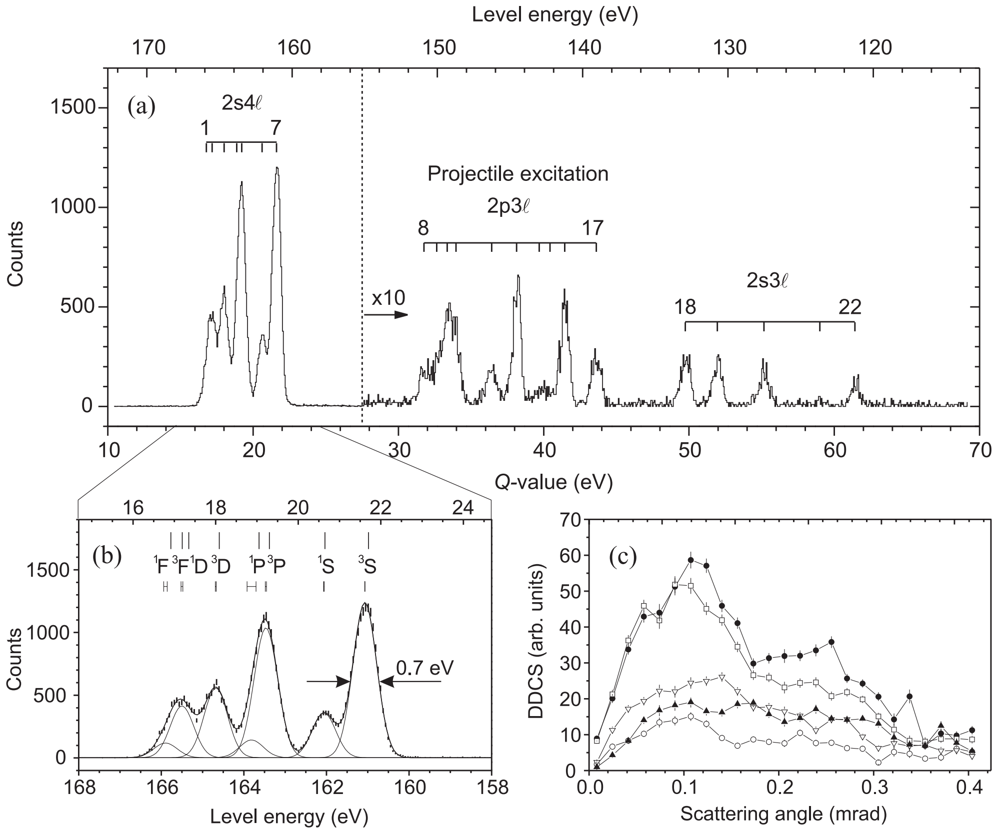

Figure 5. (a) Q-value spectrum and energy levels of Ne^{6+} following single electron capture from He at 0.355 a.u. initial velocity. For identification of energy levels 1–22 see Tab. 1. The 2p3ℓ and 2s3ℓ lines are enlarged by a factor 10. (b) Decomposition of the 2s4ℓ spectrum into different subshells and spin states. Upper marks: MCHF calculation [27]; lower marks (with error bars) exp. line positions. (c) Differential capture cross sections (arb. units) for the 2s4ℓ states: ▲, ^{1}D + ^{1,3}F; ▽, ^{3}D; □, ^{1,3}P; ○ , ^{1}S; ● , ^{3}S.

subshell levels and spin states. In total, 22 lines are observed in the Q-value spectrum (figure 5(a)), where in the case of overlapping lines a least-squares fitting procedure has been used. An example is given in figure 5(b) which shows the region of the $n = 4$ levels in more detail. The calibration of Q-values was performed by means of a linear fit of the experimental raw data (TOF values) to atomic level data from Bashkin and Stoner [24] for the most intense 2s3ℓ and 2s4ℓ lines. Energy levels relative to the ground state $1s^2 2s^2$ were derived using the known ionization energies of He and Ne^{6+}.

The observed energy levels of Ne^{6+} are identified by comparison with atomic level data [24] and recent theoretical results. These data are listed in table 1. The agreement among these results is excellent except for the 2p3p ^{1,3}S and 2p3s ^{1}P states. For 2p3p ^{1,3}S the theoretical values deviate from the present result by more than 0.5 eV. This coincides with differences among several theoretical models [25–27] for these states which are more than a factor 2 larger than for the other levels considered here. The other disagreement occurs in the atomic level data [24] for 2p3s ^{1}P and 2p3p ^{1}S with respect to the theory as well as to the present result (indicated by brackets in table 1). This discrepancy has also been mentioned previously in [26] and can be explained by the difference in identification of levels in [24].

Due to the fact that the acceptance of the spectrometer does not cover the full range of scattering angles, relative line intensities are not shown. Qualitatively, it is seen from figure 5(a) that most of the single capture events take place in the $n = 4$ shell. This is consistent with the curve-crossing model which predicts intermediate crossing radii of 8.2 to 10.8 a.u. for the 2s4ℓ states whereas the corresponding radii for the other states are significantly smaller, namely 3.8 to 5.4 a.u. for 2p3ℓ and 2.6 to 3.2 a.u. for 2s3ℓ, respectively. The decreasing crossing radii with increasing Q lead to increasing scattering angles (figure 3(b)). Here, the half Coulomb angle is indicated by the broken line.

Figure 5(b) shows the detailed spectrum of 2s4ℓ lines. All levels are identified except 2s4d ^{1}D and 2s4f ^{3}F which are not resolved. The 2s4p ^{3}P level is missing in the atomic level data [24] but has been observed very recently in a beam-foil experiment [27]. The differential cross sections for these states are shown in figure 5(c). The curves exhibit a minimum or a shoulder slightly above the half Coulomb angle around 1.5 mrad similar to Ne^{8+} (see figure 4(b)).

In future, experiments with highly charged ions extracted from the EBIT are planned where a 'reaction microscope' will be used to study multi-electron exchange accompanied with autoionization of dominantly populated highly excited projectile states. With pre-cooling of the gas jet a further increase in resolution by more than a factor 4 can be anticipated resulting in spectroscopic information on energy levels in highly charged ions not accessible by any other method.

This work was supported by the Leibniz-Program of the Deutsche Forschungsgemeinschaft. The authors would like to thank Y. Zou for helpful discussions.

Table 1. Level energies (eV) of Ne^{6+} $1s^2 2s(3\ell, 4\ell)$ and $1s^2 2p3\ell$ relative to the ground state.

Line number	Experiment: This work	Experiment: Previous data[a]	Theory[b]	Assignment
1	165.90(4)	165.77(3)[c]	165.767	2s4f ^{1}F
2	165.50(2) {	165.56(3)[c]	165.494	2s4f ^{3}F
		165.385	165.333	2s4d ^{1}D
3	164.68(1)	164.681	164.595	2s4d ^{3}D
4	163.8(1)	163.643	163.634	2s4p ^{1}P
5	163.47(1)	163.42(3)[c]	163.381	2s4p ^{3}P
6	162.061(7)	161.985	162.035	2s4s ^{1}S
7	161.069(3)	161.087	160.981	2s4s ^{3}S
8	150.93(3)	150.910	150.874	2p3d ^{1}P
9	150.04(5)	150.257	150.177	2p3d ^{1}F
10	149.32(4)	(147.913)	150.074	2p3p ^{1}S
11	148.72(3)	148.810	148.797	2p3d ^{3}P
		148.089	147.857	2p3d ^{3}D
		146.919	146.866	2p3p ^{1}D
12	146.26(2)	146.289	146.303	2p3d ^{1}D
			145.730[d]	2p3d ^{3}F
		145.348	145.369	2p3p ^{3}P
13	144.55(1)	144.573	145.190	2p3p ^{3}S
14	142.99(7)	143.323	143.273	2p3p ^{3}D
15	142.3(1)	142.417	142.419	2p3p ^{1}P
16	141.24(1)	(141.759)	141.133	2p3s ^{1}P
17	139.06(2)	139.020	139.017	2p3s ^{3}P
18	132.93(2)	132.899	132.924	2s3d ^{1}D
19	130.73(2)	130.730	130.683	2s3d ^{3}D
20	127.52(2)	127.533	127.537	2s3p ^{3}P
		127.166	127.208	2s3p ^{1}P
21	123.7(1)	123.767	123.749	2s3s ^{1}S
22	121.27(3)	121.296	121.244	2s3s ^{3}S

[a] Bashkin and Stoner [24].
[b] $2s(3\ell, 4\ell)$ levels: Hartree-Fock calculation [27], $2p3\ell$ levels: MZ code [26].
[c] recent data from [27].
[d] *R*-matrix calculation [25].

References

[1] Häberli R M, Gombosi T I, De Zeeuw D L, Combi M R and Powell K G 1997 *Science* **276** 939
[2] de Nijs A, Hoekstra R and Morgenstern R 1996 *J. Phys. B: At. Mol. Phys.* **29** 6143
[3] Tawara H, Iwai T, Kaneko Y, Kimura M, Kobayashi N, Matsumoto A, Ohtani S, Okuno K, Takagi S and Tsurubuchi S 1984 *Phys. Rev.* A **29** 1529
[4] Gaboriaud M N, Barat M, Roncin P and Sidis V 1994 *J. Phys. B: At. Mol. Phys.* **27** 4595
[5] Hasan A A, Emmons E D, Hinojosa G and Ali R 1999 *Phys. Rev. Lett.* **83** 4522
[6] Kamber E Y, Abdallah M A, Cocke C L and Stöckli M, Wang J, and Hansen J P 2000 *J. Phys. B: At. Mol. Phys.* **33** L171
[7] Mergel V, Dörner R, Ullrich J, Jagutzki O, Lencinas S, Nüttgens S, Spielberger L, Unverzagt

M, Cocke C L, Olson R E, Schulz M, Buck U, Zanger E, Theisinger W, Isser M, Geis S and Schmidt-Böcking H 1995 *Phys. Rev. Lett.* **74** 2200
[8] Dörner R, Mergel V, Spielberger L, Jagutzki O, Ullrich J and Schmidt-Böcking H 1998 *Phys. Rev.* A **57** 312
[9] Abdallah M A, Wolff W, Wolf H E, Sidky E, Kamber E Y, Stöckli M, Lin C D and Cocke C L 1998 *Phys. Rev.* A **57** 4373
[10] Abdallah M A, Wolff W, Wolf H E, Kamber E Y, Stöckli M and Cocke C L 1998 *Phys. Rev.* A **58** 2911
[11] Kamber E Y, Abdallah M A, Cocke C L and Stöckli M, 1999 *Phys. Rev.* A **60** 2907
[12] Zhang H, Fléchard X, Cassimi A, Adoui L, Cremer G, Frémont F and Hennecart D 2001 *Phys. Rev.* A **64** 012715
[13] Lubinski G, Juhsz Z, Morgenstern R and Hoekstra R 2000 *J. Phys. B: At. Mol. Phys.* **33** 5275
[14] Kamber E Y, Cocke C L, Giese J P, Pedersen J O K and Waggoner W 1987 *Phys. Rev.* A **36** 5575
[15] Kamber E Y and Ferguson S M 2001 *Phys. Rev.* A **63** 022701
[16] Niehaus A 1986 *J. Phys. B: At. Mol. Phys.* **19** 2925
[17] Olson R E 1981 *Phys. Rev.* A **24** 1726
[18] Bransden B H and McDowell M R C 1992 *Charge Exchange and the Theory of Ion-Atom Collisions* (Clarendon Press, Oxford)
[19] Beijers J P, Hoekstra R and Morgenstern R 1996 *J. Phys. B: At. Mol. Phys.* **29** 1397
[20] Beijers J P M, Hoekstra R, Schlatmann A R, Morgenstern R and de Heer F J 1992 *J. Phys. B: At. Mol. Phys.* **25** 463
[21] Beijers J P, Hoekstra R, Morgenstern R and de Heer F J 1992 *J. Phys. B: At. Mol. Phys.* **25** 4851
[22] Turksta J W, Hoekstra R, Knoop S, Meyer D, Morgenstern R and Olson R E 2001 *Phys. Rev. Lett.* **87** 123203
[23] Fléchard X, Nguyen H, Wels E, Ben-Itzhak and DePaola B D, 2001 *Phys. Rev. Lett.* **87** 123203
[24] Bashkin S and Stoner J O Jr 1978 *Atomic Energy-level and Grotrian Diagrams* (Amsterdam: North-Holland)
[25] Ramsbottom C A, Berrington K A and K L Bell 1994 *J. Phys. B: At. Mol. Phys.* **27** L811
[26] Murakami I, Safronova U I and Kato T 1999 *J. Phys. B: At. Mol. Phys.* **32** 5331
[27] Buchet-Poulizak M-C, Bogdanovich P O and Knystautas É J 2001 *J. Phys. B: At. Mol. Phys.* **34** 233
[28] Moshammer R, Unverzagt M, Schmitt W, Ullrich J and Schmidt-Böcking H 1996 *Nucl. Instrum. Methods* B **108** 425
[29] Crespo López–Urrutia J R Private communication